MATHEMATICAL BIOSCIENCES
AND ENGINEERING
Volume **2**, Number **3**, August **2005**

http://www.mbejournal.org/

pp. **643–655**

A SINGLE-CELL APPROACH IN MODELING THE DYNAMICS OF TUMOR MICROREGIONS

Katarzyna A. Rejniak

Mathematical Biosciences Institute, Ohio State University
231 West 18th Avenue, Columbus, OH 43210

Abstract. Interactions between tumor cells and their environment lead to the formation of microregions containing nonhomogeneous subpopulations of cells and steep gradients in oxygen, glucose, and other metabolites. To address the formation of tumor microregions on the level of single cells, I propose a new two-dimensional time-dependent mathematical model taking explicitly into account the individually regulated biomechanical processes of tumor cells and the effect of oxygen consumption on their metabolism. Numerical simulations of the self-organized formation of tumor microregions are presented and the dynamics of such a process is discussed.

1. **Introduction.** Most tumors in vivo arise from a single cell that has escaped the growth-controlling mechanism. However, even at very early stages of their growth, tumors become highly nonhomogeneous. Fast-growing tumor cells can significantly change their environment, leading to formation of gradients of different metabolites, such as oxygen, glucose, growth factors, and other nutrients. Changes in metabolite concentration cause in turn the development of microregions occupied by tumor cells of different phenotypes, such as proliferating, quiescent, or necrotic cells. Those subpopulations of cells are characterized by different growth and functional properties as well as by diverse responses to therapeutic factors. The biology of tumor microregions has been investigated experimentally using the multicell spheroid model (for review, see [12], [13], [19]). In an experimental setting, the spheroids are usually initiated from aggregates consisting of several cells, but as their size increases, their growth kinetics become similar to those of tumors in vivo. The multicell spheroids develop a layered structure with a central necrotic core surrounded by quiescent cells and a thin rim of proliferating cells. Steep gradients in oxygen, glucose, and other metabolites are also observed in such spheroids. Because of similarity to tumors in vivo, multicell spheroids are appropriate models to study novel antitumor therapies, and they become mandatory test systems in therapeutic screening programs (for review, see [5], [14]).

To address the formation of tumor microregions, I present a two-dimensional time-dependent mathematical model in which every tumor cell is treated as an individual entity characterized by its own geometry and individually controlled cell processes. The formation of tumor clusters and tumor microregions in this model

2000 *Mathematics Subject Classification.* 92C10, 92C37, 92C50, 76D05, 76M20.

Key words and phrases. avascular tumor growth, tumor microregions development, mathematical modeling, immersed boundary method.

depends entirely on the local dynamics of separate cells and on the cell-cell interactions. This model allows one to follow the fate of each individual cell and to investigate how changes occurring in individual cells can influence behavior of the whole tumor tissue. I have applied this model previously to study the formation of tumor clusters with random distribution of proliferating cells [16], [17]. In this paper, I extend the previous model by relating the progression of cell processes to the external sources of energy, such as oxygen, glucose, or other nutrients. For simplicity, only one external metabolic factor is introduced but the effect of its consumption on cell growth and metabolism is taken explicitly into account. Two-dimensional simulations showing the self-organized formation of the layered structure of tumor microregions occupied by cells with different phenotypes will be presented. The dynamics of microregion development will be described and compared to the experimental data.

This single-cell approach in modeling the avascular phase of tumor growth is significantly different from previous mathematical models (for review, see [1] and [9]), such as the continuum and multiphase models, which both view tumors as cell densities, and the discrete-continuous hybrid models or cellular automata models, which both view tumor cells as single points. My model allows for a more realistic representation of a single cell and individually regulated cell processes. It also allows for a more realistic representation of the tumor tissue as a conglomerate of cells nonhomogeneous in shape and function. This model is suitable for investigating those biological phenomena that occur on the scale ranging from one to several hundreds of cells. Therefore, it can be used to bridge research conducted on different scales. Results of intracellular research can serve as a source of parameters employed in my model, and similarly, results obtained from this model can be used in defining attributes of the large-scale approaches, such as the hybrid-type or continuum models.

2. **Mathematical formulation.** My mathematical model is based on the immersed boundary method [15] and captures interactions between immersed elastic tumor cells and a viscous incompressible fluid, representing the cytoplasm inside the cells and the extracellular matrix outside the tumor tissue. The fluid flow is influenced by sources of fluid located inside the growing cells, as well as by forces generated by the immersed, elastic boundaries, while at the same time the elastic structures move at the local fluid velocity. The cell cycle and cell processes are related to the concentration of external factors, such as oxygen, sensed by the cell from its local environment.

This model is defined on the square two-dimensional domain Ω. The elastic membranes of the tumor cells form a collection Γ of closed curves defined in the curvilinear coordinates $\mathbf{X}(l,t)$, where l is a position along the cell boundary. The fluid inside and outside the cells is modeled as a homogeneous continuum with the same constant density ρ and viscosity μ. The cell nuclei are represented by a finite set Ξ of discrete material points $\mathbf{Y}_k$ in which sources of fluid $S_k(t)$ are located if the host cells are growing. This is a simplification of the biological process in which the required fluid is recruited from the extracellular matrix through the cell membrane, but this choice for the location of fluid sources is not critical for the computational results. Oxygen concentration $\gamma(\mathbf{x},t)$ is defined in a domain that coincides with the fluid domain. The rate of change of oxygen concentration depends on oxygen consumption by the tumor cells and on its diffusion. The complete system of

equations describing the interaction between tumor cells, the extracellular matrix and concentration of oxygen is given in equations (1)–(9).

$$\rho\left(\frac{\partial \mathbf{u}(\mathbf{x},t)}{\partial t} + (\mathbf{u}(\mathbf{x},t)\cdot\nabla)\mathbf{u}(\mathbf{x},t)\right) = -\nabla p(\mathbf{x},t) + \mu\Delta\mathbf{u}(\mathbf{x},t) + \frac{\mu}{3\rho}\nabla s(\mathbf{x},t) + \mathbf{f}(\mathbf{x},t), \tag{1}$$

$$\rho\nabla\cdot\mathbf{u}(\mathbf{x},t) = s(\mathbf{x},t), \tag{2}$$

$$\mathbf{f}(\mathbf{x},t) = \int_\Gamma \mathbf{F}(l,t)\ \delta(\mathbf{x}-\mathbf{X}(l,t))\ dl, \tag{3}$$

$$s(\mathbf{x},t) = \sum_{k\in\Xi} S_k(t)\ \delta(\mathbf{x}-\mathbf{Y}_k(t)), \tag{4}$$

$$\frac{\partial \mathbf{X}(l,t)}{\partial t} = \mathbf{u}(\mathbf{X}(l,t),t) = \int_\Omega \mathbf{u}(\mathbf{x},t)\ \delta(\mathbf{x}-\mathbf{X}(l,t))\ d\mathbf{x}, \tag{5}$$

$$\frac{\partial \mathbf{Y}_k(t)}{\partial t} = \mathbf{u}(\mathbf{Y}_k(t),t) = \int_\Omega \mathbf{u}(\mathbf{x},t)\ \delta(\mathbf{x}-\mathbf{Y}_k(t))\ d\mathbf{x}, \tag{6}$$

$$\mathbf{F}(l,t) = \mathcal{F}(\mathbf{X}(l,t),t), \tag{7}$$

$$S_k(t) = \mathcal{S}(\gamma(\mathbf{Y}_k,t),t), \tag{8}$$

$$\frac{\partial \gamma(\mathbf{x},t)}{\partial t} = \mathcal{D}_\gamma\ \Delta\gamma(\mathbf{x},t) - V_\gamma\ \frac{\gamma(\mathbf{x},t)}{\kappa_\gamma+\gamma(\mathbf{x},t)}\cdot\chi(\Theta_\Gamma), \tag{9}$$

$$\gamma(\mathbf{Y}_k,t) = \int_\Omega \gamma(\mathbf{x},t)\ \delta(\mathbf{x}-\mathbf{Y}_k(t))\ d\mathbf{x}. \tag{10}$$

In this system, equations (1)–(2) are the Navier-Stokes equations of a viscous incompressible fluid. Equation (1) is Newton's second law, where mass density times the material acceleration is equal to the sum of various force densities arising from the fluid pressure p, the viscosity μ, the local fluid expansion s, and the external force $\mathbf{f}$. Equation (2) is the law of mass conservation, where the source distribution s is identically equal to zero on the whole fluid domain except at the isolated point sources that are used to model the growth of cells. The conservation of mass must be preserved globally in the fluid domain Ω at each time t; that is, $\rho\int_\Omega(\nabla\cdot\mathbf{u})\ d\mathbf{x} = 0$.

Equations (3)–(6) represent interactions between the fluid and the immersed points of cell boundaries and cell nuclei. In equations (3)–(4), the force density defined on cell boundaries and sources defined at the cell nuclei are applied to the fluid, while in equations (5)–(6) all material points are carried along with the fluid. The Dirac delta function in these equations is two dimensional; thus $\delta(\mathbf{x}) = \delta(x_1)\cdot\delta(x_2)$.

Equation (7) states that the boundary force $\mathbf{F}(l,t)$ is determined by the boundary configuration at time t, where the function $\mathcal{F}$ satisfies a generalized Hooke's law. The boundary forces include the adjacent, adhesion, and contractile forces and will be described below. Equation (8) states that the source strength $S_k(t)$ at time t is determined by the oxygen concentration around the nucleus of a growing cell $\mathbf{Y}_k$, where the function $\mathcal{S}$ is a step function that takes nonzero values only during the time of cell growth. To satisfy conservation of mass globally, the balancing sinks of fluid are located at the fixed positions on the domain boundary.

Equation (9) is a diffusion-reaction equation defining the rate of change of oxygen concentration γ. It is assumed that oxygen is not carried with the moving cytoplasm and its dynamics comes only from its diffusion and consumption modeled using the Michaelis-Menten formulation. The biological process of oxygen sensing and oxygen

consumption is quite complex, but it is simplified in this model by assuming that both processes take place near the boundaries Γ of tumor cells, that is within the cell microenvironment Θ_Γ (here χ is a set characteristic function). The choice of cell membranes for the site of oxygen sensing and oxygen consumption is not critical for the computational results.

Equation (10) states that oxygen concentration at the material point $\mathbf{Y}_k$ is equal to the local concentration of oxygen around that point.

2.1. **Cell structure.** A eukaryotic cell is represented by a discrete collection of moving points $\{\mathbf{X}_l(t)\}$ that form the elastic plasma membrane and enclose the fluid cytoplasm and the point nucleus located inside the cell. The elasticity of the plasma membrane comes from the fact that each point $\mathbf{X}_l(t)$ on the cell boundary is connected to its two adjacent neighboring points $\mathbf{X}_{l+1}(t)$ and $\mathbf{X}_{l-1}(t)$ by a linear spring $\mathbf{F}_{adj}$, satisfying Hooke's law with the constant resting length $\mathcal{L}_{adj}$ and constant spring stiffness $\mathcal{F}_{adj}$:

$$\mathbf{F}_{adj}(l,t) \;=\; \sum_{k=l-1,l+1} \mathcal{F}_{adj} \;\frac{\|\mathbf{X}_k(t)-\mathbf{X}_l(t)\|-\mathcal{L}_{adj}}{\|\mathbf{X}_k(t)-\mathbf{X}_l(t)\|}\;\left(\mathbf{X}_k(t)-\mathbf{X}_l(t)\right). \tag{11}$$

2.2. **Cell-cell adhesion.** Separate cells can adhere to their neighbors by using the transmembrane adhesion proteins, which are represented as short linear springs attached at the boundary points $\mathbf{X}_l(t)$ and $\mathbf{X}_k(t)$ of two distinct cells if they are within the distance $\mathcal{L}^{max}_{adh}$. The adhesive force $\mathbf{F}_{adh}$ satisfies Hooke's law with the constant resting length $\mathcal{L}_{adh}$ and constant spring stiffness $\mathcal{F}_{adh}$:

$$\mathbf{F}_{adh}(l,t) \;=\; \mathcal{F}_{adh}\;\frac{\|\mathbf{X}_k(t)-\mathbf{X}_l(t)\|-\mathcal{L}_{adh}}{\|\mathbf{X}_k(t)-\mathbf{X}_l(t)\|}\,\left(\mathbf{X}_k(t)-\mathbf{X}_l(t)\right), \tag{12}$$

provided $\|\mathbf{X}_k(t)-\mathbf{X}_l(t)\| \le \mathcal{L}^{max}_{adh}$ and is zero otherwise. Note that this equation also represents a repulsive force if the distance between cell boundaries is smaller than $\mathcal{L}_{adh}$.

Figure 1 shows a small cluster of eukaryotic cells with boundary points (stars), cell nuclei (circles), linear springs between adjacent boundary points (thin lines), and adhesive connections between distinct cells (thick lines).

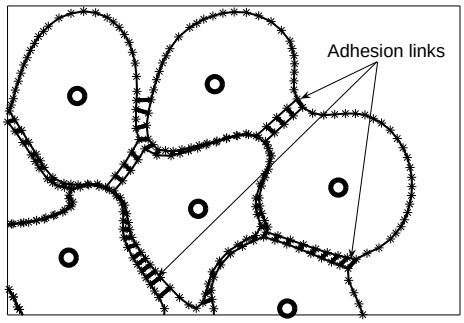

FIGURE 1. A cluster of eukaryotic cells connected by adhesive links. Each cell consists of the nucleus (circle) enclosed by the plasma membrane (stars) connected by linear adjacent springs (thin lines) and linear adhesive links (thick lines).

2.3. **Cell microenvironment.** All boundary points located on the membrane Γ_k of the kth cell play an additional role of cell membrane receptors. They are used by the cell to sense concentration of oxygen from the cell microenvironment $\Theta_{\Gamma_k} = \bigcup_{\mathbf{X}\in\Gamma_k} \{\mathbf{x} : ||\mathbf{x} - \mathbf{X}|| < \varepsilon\}$ defined as a set of points lying within a distance ε from the cell boundary Γ_k.

2.4. **Cell life cycle.** All cells are considered viable and ready for proliferation unless the concentration of oxygen in the cell microenvironment falls below a certain level γ_{min}, when the cell loses its ability to proliferate and becomes necrotic. All viable and proliferating cells consume oxygen dissolved in their microenvironments at a rate that is relatively independent of oxygen concentration until very low oxygen levels are reached. At such concentrations, the rate of oxygen consumption decreases with decreasing oxygen concentration [3]. This process is modeled in equation (9) by using the Michaelis-Menten formulation. All necrotic cells remain inside the tumor cluster but stop participating in oxygen consumption. Since it is observed in the tumor multicell spheroids growing in vitro that less than 10% of all viable cells are mitotically active, not all viable cells in this model will start growing immediately. In fact, a process of cell proliferation is initiated periodically (at time intervals corresponding to 15 minutes) in such a viable cell that senses the highest level of oxygen in its vicinity. The quiescent cells are capable of proliferation but do not participate in the mitotic process, because they experience a lower concentration of oxygen in their microenvironment than other cells in the cluster.

2.5. **Cell proliferation.** A process of cell proliferation is modeled by introducing two point sources inside the cell that correspond to two sets of sister chromatids (Fig. 2a). These sources are located along the cell's longest axis. The fluid created by both sources causes cell growth by pushing cell boundaries and by increasing the cell area (Fig. 2b). The sources are deactivated when the cell area is doubled. At this time, two opposite points on the cell boundary are selected in such a way that a line provided between them separates the cell into two parts of approximately equal areas, each with its own nucleus (former point sources). The contractile ring is created by attaching the contractile forces to the opposite points on the cell boundary. This results in a formation of the contractile furrow (Fig. 2c) and causes division of the cell into two daughter cells (Fig. 2d). More details on the process of cell division can be found in [17].

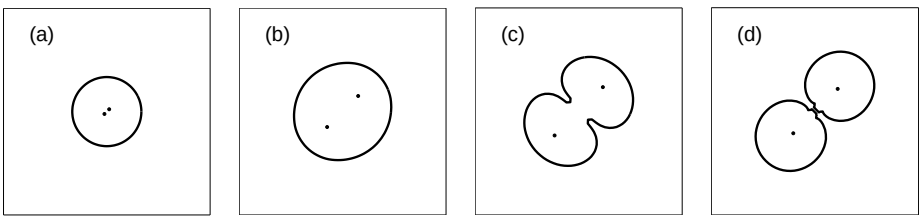

FIGURE 2. Main phases of the cell cycle: (a) nucleus division, (b) cell growth and elongation, (c) formation of the contractile ring, (d) cellular division and formation of two daughter cells.

The strength of each fluid source $S_k(t)$ is a step function that takes a nonzero value $\mathcal{S}_0$ over the time of cell growth, but once the cell area is doubled, the fluid

sources are deactivated. The value of $\mathcal{S}_0$ is determined computationally or experimentally to match dynamics of the growing living cell.

The contractile forces $\mathbf{F}_{div}$ are defined between two opposite boundary points $\mathbf{X}_l(t)$ and $\mathbf{X}_k(t)$ of the same cell. They act on the cell boundaries until the opposite points reach a distance $\mathcal{L}_{div}^{min}$, at which point the dividing cell splits into two daughter cells. Each contractile force satisfies Hooke's law with the constant resting length $\mathcal{L}_{div}$ and constant spring stiffness $\mathcal{F}_{div}$:

$$\mathbf{F}_{div}(l,t) \;=\; \mathcal{F}_{div}\;\frac{\|\mathbf{X}_k(t)-\mathbf{X}_l(t)\|-\mathcal{L}_{div}}{\|\mathbf{X}_k(t)-\mathbf{X}_l(t)\|}\left(\mathbf{X}_k(t)-\mathbf{X}_l(t)\right), \tag{13}$$

provided $\|\mathbf{X}_l(t)-\mathbf{X}_k(t)\| \geq \mathcal{L}_{div}^{min}$ and is zero otherwise. The value of the spring stiffness constant $\mathcal{F}_{div}$ is determined computationally in a way that resembles the dynamics of cytokinesis in the living cell.

3. **Numerical implementation.** This model is implemented by using the finite difference schemes for discretizing the Navier–Stokes equations and the reaction-diffusion equation. The same regularly spaced fluid and oxygen grid is used. Interactions between those grids and the material points on cell boundaries and at cell nuclei are implemented using the discrete approximation $\delta_h(\mathbf{x})$ to the Dirac delta function, where $\delta_h(\mathbf{x}) = \delta_h(x_1)\cdot\delta_h(x_2)$ and

$$\delta_h(r) = \begin{cases} \frac{1}{4h}\,\left(1+cos(\frac{\pi r}{2h})\right) & \text{if} \quad |r|<2h, \\ \\ 0 & \text{if} \quad |r|\geq 2h. \end{cases} \tag{14}$$

3.1. **Algorithm.** The numerical algorithm for the full coupled system can be outlined as follows. At the end of time step n, we are given values of the fluid velocity field $\mathbf{u}^n$, the concentration of oxygen γ^n, the configuration of the immersed boundary points $\mathbf{X}^n$ on the cell membranes, and the positions of cell nuclei $\mathbf{Y}^n$. These values are updated at the next time step in the following way:

1. Inspect the concentration of oxygen γ^n in the microenvironments of all quiescent cells to determine which cells become necrotic; inspect all quiescent cells to determine which of them is exposed to the highest level of oxygen and will start growing; update the levels of oxygen concentration γ^{n+1} by computing rates of its consumption in the vicinity of all quiescent and proliferating cells.
2. Determine the source distribution S^n at the nuclei of growing cells and the balancing sinks at the boundary of fluid domain; spread these values to the neighboring grid points to find the local growth rate s^n of the fluid.
3. Calculate the total force density $\mathbf{F}^n$ at the cell boundaries, including the membrane adjacent forces, cell-cell adhesion forces, and contractile forces in the dividing cells; spread those values to the neighboring grid points to determine the forces $\mathbf{f}^n$ on the fluid.
4. Solve the Navier–Stokes equations for the fluid velocity field $\mathbf{u}^{n+1}$ by using the fast Fourier algorithm.
5. Interpolate the fluid velocity field $\mathbf{u}^{n+1}$ to each immersed boundary point on cell membranes and to each cell nuclei; compute new positions of material points $\mathbf{X}^{n+1}$ and $\mathbf{Y}^{n+1}$ by moving them at the local fluid velocity using a forward Euler step.

More details about a numerical implementation of this algorithm and the numerical solution of the Navier-Stokes equations, can be found in [18] and [16].

3.2. **Choice of computational parameters.** My model of growing tumors is defined on a two-dimensional square domain corresponding to the tissue of size 0.7mm × 0.7mm. This domain is discretized using the 512 × 512 grid, which gives the mesh width $h = 1.37\mu$m. The nonproliferating tumor cells have diameters of 10μm. Resting lengths of all adjacent $\mathcal{L}_{adj}$, adherent $\mathcal{L}_{adh}$, and contractile springs $\mathcal{L}_{div}$ are equal to the half of mesh width $h/2$, whereas radii ε of all adhesion $\mathcal{L}_{adh}^{max}$, contractile $\mathcal{L}_{div}^{min}$, and oxygen-sensing microenvironments are equal to the mesh width, h. The time step used in all simulations is equal to $\Delta t = 0.001$ seconds.

Fluid viscosity and density have been chosen to reflect the rheological properties of the network part of the cytoplasm as reported in [10] and [4]. Stiffness of the adjacent springs in the cell membrane corresponds to rigidity of the cortical cytoskeletal network associated with the plasma membrane [10]. Stiffness of the adherent connections in normal cells has been reported in [2]; however, a smaller value has been chosen for all computations, since the tumor cells are known to have weaker adhesion connections than those in normal cells. Strength of sources in the growing cells and stiffness of the contractile forces have been determined computationally in my previous work [16] to match the dynamics of growing and dividing cells, respectively. The values of oxygen concentration and consumption rates have been reported in the series of experimental papers on the in vitro growth of the multicell spheroids [3], [6], [7], [8]. The value of oxygen diffusion in the living tissues has been reported in [20]. The values of all physical parameters are summarized in Table 1.

TABLE 1. Numerical values of computational parameters

Physical quantity	Computational parameter			References
fluid viscosity	μ	=	$100\ g/(cm \cdot s)$	[10]
fluid density	ρ	=	$1.35\ g/cm^3$	[4]
source strength	$\mathcal{S}_0$	=	$2 \times 10^{-7}\ g/s$	[16], [17]
stiffness of adjacent springs	$\mathcal{F}_{adj}$	=	$500\ g/(cm \cdot s^2)$	[10]
stiffness of adherent springs	$\mathcal{F}_{adh}$	=	$100\ g/(cm \cdot s^2)$	[2]
stiffness of contractile springs	$\mathcal{F}_{div}$	=	$5 \times 10^7\ g/(cm \cdot s^2)$	[16], [17]
optimal oxygen concentration	γ_0	=	$0.28\ mM$	[6], [7], [8]
max oxygen consumption rate	V_γ	=	$2.36 \times 10^{-7}\ g/(cm^3 \cdot s)$	[6], [7], [8]
Michaelis constant	κ_γ	=	$0.046\ mM$	[3]
necrotic oxygen level	γ_{min}	=	$0.0082\ mM$	[3]
diffusion coefficient	$\mathcal{D}_\gamma$	=	$10^{-6}\ cm^2/s$	[20]

4. **Computational results.** Initially, a small cluster of seven viable tumor cells is placed at the center of the computational domain filled uniformly with oxygen of optimal concentration γ_0. Periodically (about every 15 minutes), the process of proliferation is started by a viable cell with the highest concentration of oxygen in its vicinity. The tumor cell grows until its area is doubled; then it is divided into two daughter cells. All viable and proliferating cells consume oxygen dissolved in their environment. If oxygen concentration falls below the γ_{min} level in the vicinity of a viable cell, this cell becomes necrotic. Therefore, the fate of each tumor cell depends entirely on the evolution of oxygen concentration in the cell microenvironment. All computer simulations have been carried over the period corresponding to 14 days of tumor development. The results discussed below show formation of tumor microregions occupied separately by cells with different phenotypes and characterized by different concentrations of oxygen.

4.1. **Dynamics of tumor growth.** The dynamics of tumor growth over the period of 14 days is summarized in Figure 3 by presenting the evolution of a tumor area and the development of three subpopulations of tumor cells—proliferating, quiescent, and necrotic. My model predicts fast expansion of a cluster of tumor cells during the first 4–5 days and significant reduction in tumor growth after that time. Finally, during the last 2–3 days, the tumor cluster enters into a phase of growth saturation, (Fig. 3a).

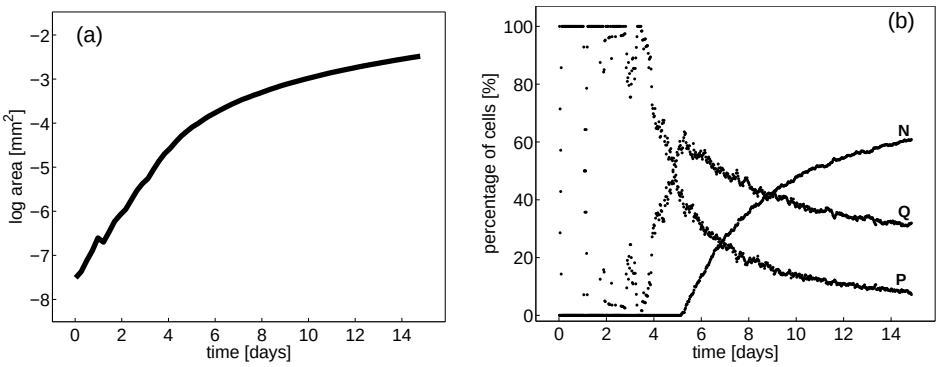

FIGURE 3. Dynamics of tumor growth. (a) Three-phased evolution of the tumor area—fast expansion, growth reduction, and growth saturation. (b) Development of tumor-cell subpopulations—percentage of necrotic (N), quiescent (Q), and proliferating (P) cells in the whole tumor cluster.

The initial fast tumor growth follows from the fact that almost all tumor cells proliferated actively during the first four days. The percentage of proliferating tumor cells is equal to 100% during this time, except for the scattered single points that reflect short periods of time, when the newly created daughter cells did not yet enter in the new cell cycle, (Fig. 3b). A subpopulation of quiescent cells becomes more noticeable after the third day of tumor development and reaches the maximal capacity of 65% at the time when the first necrotic cells arise. After this time, the percentage of quiescent cells decreases to about 40% on the fourteenth day. A subpopulation of necrotic cells arises first around the fifth day of tumor growth and is characterized by a fast exponential expansion. The percentage of proliferating cells starts to decrease with the increasing subpopulations of quiescent and necrotic cells. It reaches less than 10% of all tumor cells at the end of the fourteenth day. This general pattern in formation of subpopulations of tumor cells, predicted by my model, is consistent with results of biological experiments reported in [6], [7], [8], [12]. In particular, Figure 3a corresponds to prevascular tumor growth shown in Figure 2 of [12].

4.2. **Spatial distribution of tumor cell subpopulations.** Figure 3b presents the temporal evolution of tumor microregions, while the spatial distribution of emerging tumor-cell subpopulations over the same period of 14 days is shown in Figure 4. My model predicts that initially the distribution of proliferating cells is uniform in the whole tumor cluster. This follows from the fact that the cluster is small, so every cell is exposed to a relatively large oxygen concentration and it will start growing at some point. After about four days, however, the populations of

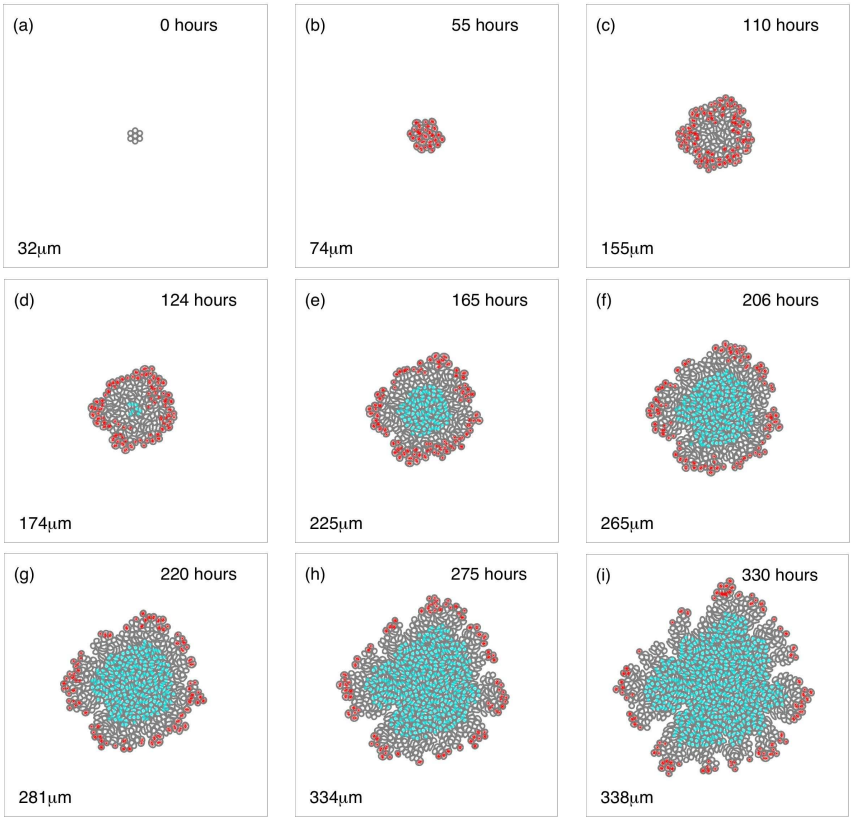

FIGURE 4. Spatial development of three tumor microregions containing proliferating cells (red), necrotic cells (blue), and quiescent cells (gray). Time of growth and tumor diameters are shown.

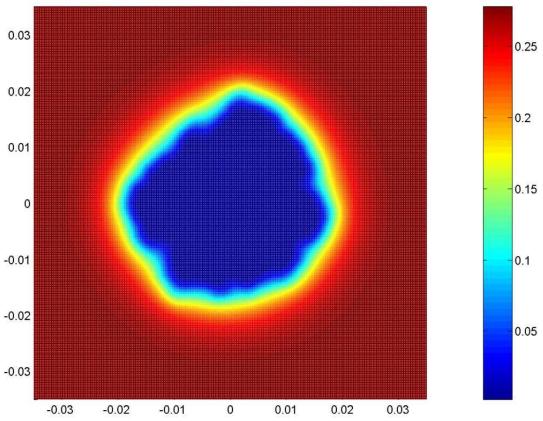

FIGURE 5. Distribution of oxygen concentration after 14 days of tumor development corresponding to the shape of the tumor cluster shown in Figure 4i. Oxygen concentration measured in mM, distance in cm.

quiescent and proliferating cells become spatially separated. The outer rim of actively mitotic cells is formed, while the quiescent cells occupy the center of the cluster. The formation of an inner layer of quiescent cells is a result of cluster size and oxygen depletion. Since only the cells with the highest concentration of oxygen in their microenvironment start growing, the cells located closer to the cluster surface proliferate more often. The quiescent cells located inside the cluster can enter the growing phase only if all cells exposed to a higher oxygen concentration are already proliferating. Of course, with the increasing size of the tumor, the number of cells located close to the tumor surface is larger, and cells located inside the cluster are less likely to start proliferating. The first necrotic cells arise in the center of the tumor cluster after five days of its growth. Further development leads to the expansion of the necrotic core, while the surrounding layer of quiescent cells has a relatively stable radius—around 48-50μm (Figs.4f–h). The outer rim of proliferating cells has a width of a few tumor cells. These predictions of my model are consistent with other biological experiments [6], [7], [8], [11]. In particular, the three-layered structure of the multicell spheroid is shown in Figure 2 of [11].

4.3. **Development of oxygen gradients.** The spatial distribution of tumor-cell subpopulations depends on oxygen concentration sensed by the cells from their microenvironment. Initially, this concentration is uniformly equal to 0.28mM, however, extensive oxygen consumption by the quickly growing tumor cells creates a steep gradient of oxygen in the tumor tissue and its surroundings. Figure 5 shows the spatial distribution of oxygen concentration after 14 days of tumor development that corresponds to the shape of the tumor cluster presented in Figure 4i. The dark blue region in the center of the domain corresponds to the area of high oxygen reduction (concentration of less than 0.01mM) where the necrotic tumor cells are located. The dark red region far from the tumor cluster contains oxygen of high concentration (more than 0.25mM). The pronounced gradient of oxygen is visible around the rim of proliferating cells (the green yellow region). Representative profiles of oxygen concentration taken at four different time points during the tumor development are shown in Figure 6.

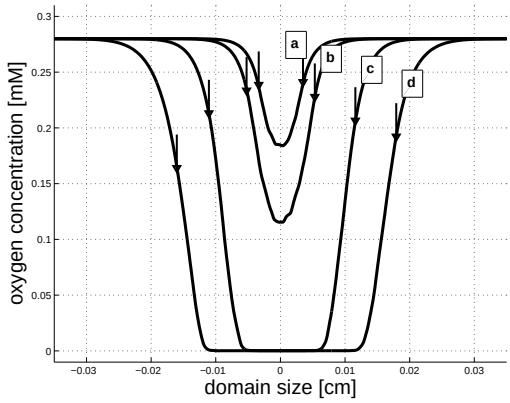

FIGURE 6. Profiles of oxygen concentration in tumor clusters of four sizes: (a) diameter of 74μm, 2 days of tumor growth; (b) 109μm, 3 days; (c) 225μm, 6 1/2 days; (d) 334μm, 11 1/2 days.

These profiles are captured along a horizontal line crossing the center of the domain. All profiles are characterized by decreased oxygen concentration in the region directly surrounding the tumor cluster, thus lowering the concentration of oxygen at the tumor surface (indicated by vertical arrows in Fig.6). In small tumor clusters, the shapes of oxygen profiles are parabolic (graphs a and b in Fig.6). In larger clusters, gradients are steeper and show a central plateau with a near-zero concentration of oxygen (graphs c and d in Fig.6). The profiles of oxygen concentration presented in Figure 6 are analogous to the profiles of partial oxygen pressure in multicell spheroids discussed in [11] and [12]. Since those two quantities are proportional by Henry's law, all predictions of my model are consistent with biological experiments.

5. **Discussion.** I have presented a new, single-cell approach in modeling the formation and development of tumor microregions. The novelty of my model lies in treating every cell as a separate entity with its own geometry and individually regulated cell processes. Development of the whole tumor cluster is a result of local dynamics of separate growing cells that need to compete for space and resources with their neighbors. This model takes explicitly into account the effect of oxygen consumption on cell metabolism. It also includes the effects of cell-cell interactions on the geometry of separate cells and the whole tumor tissue.

I have applied this model in numerical simulations of the oxygen-dependent growth of tumor clusters that can be considered as models for micrometastatic or avascular primary tumors. I have shown that predictions of my model regarding the dynamics of tumor growth, the emergence of tumor-cell subpopulations, the temporal and spatial evolutions of tumor microregions, and the profiles of oxygen concentration are all biologically adequate.

This approach allows one to follow the fate of a single tumor cell in the cluster or the whole clone of cells arising from a common predecessor. As an illustrative example, I present the evolution of seven color-coded clones emerging from single cells shown in Figure 7a. The final configuration of separate clones, containing about 900 cells in total, is presented in Figure 7b.

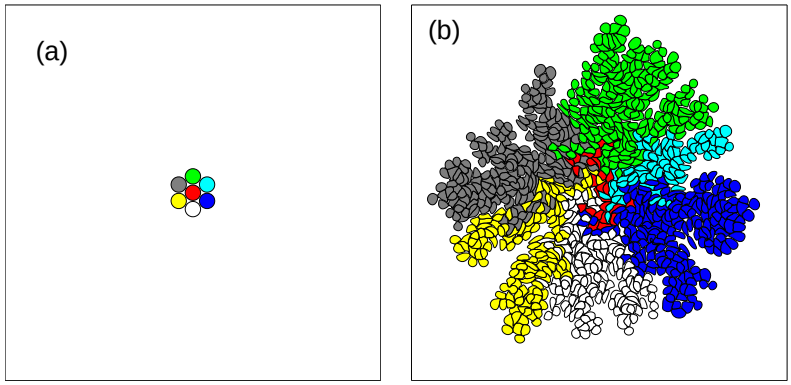

FIGURE 7. Seven color-coded predecessor cells (a) give rise to asymmetrically developed clones shown after 14 days of tumor growth (b).

Note that the red clone in Figure 7b is in extinction, because it has emerged from a centrally located predecessor cell, and because of this location, all red cells

need to compete for space and oxygen with all other clones. Six other clones have arisen from symmetrically located predecessor cells; however, they did not develop uniformly. Some of them have been dominated by their neighbors during the tumor growth, such as the light blue clone that probably will not survive during further development of the tumor cluster. This asymmetry in clonal development follows from the fact that cells with higher concentrations of oxygen in their vicinity proliferate more often, allowing tumor cells to spread widely in search of well-oxygenated environments. Since the oxygen concentration is depleted in the regions densely occupied by tumor cells, the growing cluster tends to form arms directed toward the regions rich in oxygen. Therefore the cells located on the cluster boundary are more likely to start proliferation and to penetrate the surrounding area. This may be an indication of tumor aggressiveness. The more symmetrical shape of the cluster can be achieved by changing some parameters in the model.

The possibility of observing a lifespan of each separate cell and the fate of all its daughter cells in many succeeding generations gives an opportunity to model the biomechanical consequences of cell genetic mutations. By altering properties of a single cell or of a small group of cells (for instance, the cell doubling time can be shortened or elongated, cell resistance to hypoxia can be altered, or cell-cell adherent connections can be loosened or strengthened), and assuming that all daughter cells will carry on those genetic mutations, we can observe changes in the tumor growth and its responses to the external factors.

I have presented here a very simple situation with only one source of energy regulating the life of each tumor cell, whereas biological processes in living cells involve not only oxygen concentration but also other metabolites, such as glucose, lactic acid or pH. In further research, I plan to investigate the growth of tumors taking into account cell behavior in more complex environments and cell responsiveness to more than one metabolic factor.

This model also allows for investigation of other biological phenomena occurring on the scale of one to several hundreds of cells. It can be used as an intermediate model between the intracellular and large-scale models. Results of intracellular research can serve as sources of parameters employed in this model, and similarly, results obtained from this model can be used in defining attributes of the large-scale approaches, such as the hybrid-type or continuum models. Therefore, the computation approach presented in this paper can bridge the micro- and macroscale models.

Acknowledgments. I thank Magdalena M. Musielak for her critical reading of this manuscript. All computations have been performed on the OSC Intel Pentium 4 Xeon cluster at the Ohio Supercomputer Center. This work has been supported by the NSF under agreement no. 0112050.

REFERENCES

[1] R. P. Araujo and D. L. S. McElwain, A history of the study of solid tumor growth: The contribution of mathematical modelling, Bull. Math. Biol. 65 (2004), 1039–1091.
[2] G. I. Bell, Models for specific adhesion of cells to cells, Science 200 (1978), 618–627.
[3] J. J. Casciari, S. V. Sotirchos and R. M. Sutherland, Variations in tumor cell growth rates and metabolism with oxygen concentration, glucose concentration, and extracellular pH, J. Cell. Physiol. 151 (1992), 386–394.
[4] M. Dembo and F. Harlow, Cell motion, contractile networks, and the physics of interpenetrating reactive flow, Biophys. J. 50 (1986), 109–121.

[5] C. Dubessy, J-L. Merlin, C. Matchal and F. Guillemin, Spheroids in radiobiology and photodynamic therapy, Critical Reviews in Oncology/Hematology 36 (2000), 179–192.
[6] J. P. Freyer and R. M. Sutherland, A reduction in the in situ rates of oxygen and glucose consumption of cells on EMT6/Ro spheroids during growth, J. Cell Physiol. 124 (1985), 516–524.
[7] J. P. Freyer and R. M. Sutherland, Regulation of growth saturation and development of necrosis in EMT6/Ro multicellular spheroids by the glucose and oxygen supply, Cancer Research 46 (1986), 3513–3520.
[8] J. P. Freyer and R. M. Sutherland, Proliferative and clonogenic heterogeneity of cells from EMT6/Ro multicellular spheroids induced by the glucose and oxygen supply, Cancer Research 46 (1986), 3504–3512.
[9] A. Friedman, A hierarchy of cancer models and their mathematical challenges, Discrete and Continuous Mathematical Systems—Series B 4 (2004), 147–159.
[10] V. M. Laurent, E. Planus, R. Fodil and D. Isabey, Mechanical assesment by magnocytometry of the cytostolic and cortical cytoskeletal compartments in adherent epithelial cells, Biorheology 40 (2003), 235–240.
[11] W. F. Mueller-Klieser and R. M. Sutherland, Oxygen tension in multicellular spheroids of two cell lines, Br. J. Cancer 45 (1982), 256–264.
[12] W. Mueller-Klieser, Multicellular spheroids. A review on cellular aggregates in cancer research, J. Cancer Res. Clin. Oncol. 113 (1987), 101–122.
[13] W. Mueller-Klieser, Three-dimensional cell cultures: From molecular mechanisms to clinical applications, Am. J. Physiol. 273 (1997), C1109–C1123.
[14] W. Mueller-Klieser, Tumor biology and experimental therapeutics, Critical Reviews in Oncology/Hematology 36 (2000), 123–239.
[15] C. Peskin, The immersed boundary method, Acta Numerica, 11 (2002), 479–517.
[16] K. A. Rejniak, Modeling formation of solid tumors with discrete viscoelastic cells, SIAM J. Sci. Computing, (submitted to).
[17] K. A. Rejniak, An immersed boundary model of the formation and growth of solid tumors, Technical Report 19 (2004), MBI, Ohio State University, http://mbi.osu.edu/publications/techreport%2019.pdf
[18] K. A. Rejniak, H. J. Kliman and L. J. Fauci A computational model of the mechanics of growth of the villous trophoblast bilayer, Bull. Math. Biol. 66 (2004), 199–232.
[19] R. M. Sutherland, Cell and environment intreractions in tumor microregions: The multicell spheroid model, Science 240 (1988), 177–184
[20] E. A. Swabb, J. Wei and P. M. Gullino, Diffusion and convection in normal and neoplastic tissue, Cancer Research 34 (1974), 2814–2822

Received on January 1, 2005. Revised on June 8, 2005.

E-mail address: rejniak@mbi.osu.edu